The Mathematics of the Imaging Techniques of MEG, CT, PET and SPECT

A.S. Fokas, V. Marinakis

Department of Applied Mathematics and

Theoretical Physics, University of Cambridge

Cambridge, CB3 0WA, United Kingdom

Abstract

The imaging techniques of magnetoencephalography (MEG), of computed tomography (CT), of positron emission tomography (PET) and of single photon emission computed tomography (SPECT) are reviewed, and the analytical solutions of the relevant inverse problems are presented. The numerical implementation of the exact formulas yield accurate reconstructions for both realistic phantoms as well as real data.

1 Introduction

We first present a brief review of magnetoencephalography (MEG), as well as of the emission techniques of positron emission tomography (PET) and of single photon emission computed tomography (SPECT).

MEG is a non invasive technique that can be used to investigate brain activity. When neurons are active they produce small currents whose basis is the change in the concentration of certain ions (ionic currents) [Hille, 1992]. The flow of current in the neural system produces a weak magnetic field. The measurement of this field outside the brain and the estimation of the current density distribution that produced this field is called MEG. Neuromagnetic signals are typically 50–500fT, which are of the order of 10^{-9} of the earth's geomagnetic field. Currently, the only detector that can measure these tiny fields is the superconducting quantum interference device (SQUID). The main advantage of MEG over other functional imaging techniques, such as PET, SPECT and functional magnetic resonance imaging (fMRI), is that it has better time resolution. The time resolution of the former techniques is of the order of 1s, whereas that of MEG is of the order of 10ms. This is a crucial factor if one wants to study brain dynamics. For example, in the book of G. Edelman and G. Tononi, "A universe of consciousness: how matter becomes imagination", only data from MEG are used [Edelman & Tononi, 2000]. The main difficulty with MEG is the lack of uniqueness, namely there exist *many* currents which give rise to the same magnetic field. Although this fact was already known to Helmholtz since 1853 [Helmholtz, 1853], it was not known until our work, *exactly which part of the current can be determined by measuring the magnetic field outside the brain.* We have recently answered completely this question for the case that the brain can be approximated by a sphere [Fokas et al., 1996]: We have found that the only part of the current that can be determined from the measurements consists of certain moments of one of the two functions specifying the tangential part of the current (the other function specifying the tangential part of the current as well as the radial part of the current cannot be determined). Furthermore, in addition to the above "negative" result we have also obtained the following "positive" result: *If one assumes that the current is such that the energy norm is minimized, then the current can be uniquely determined from the measurements.*

We have implemented the formula for the minimizing current numerically [Fokas et al., 2004a] and our results are currently being tested at the Department of Neurosurgery, University of Texas Medical School. Preliminary results indicate that our new algorithm gives more accurate results than the standard dipole models used so far.

PET and SPECT are two modern imaging techniques with a wide range of medical applications. Although these techniques were originally developed for the study of the *functional* characteristics of the brain, they are now used in many diverse areas of clinical medicine [Andreasen, 1997; Bengel et al., 2001; Doubrovin et al., 2001; Green et al., 2002; Hutton, 1997; Jonides et al., 1996; Junck et al., 1989; Lardinois et al., 2003; Lauritzen & Olesen, 1984; Lee et al., 1988; Mark et al., 1996; Mazziotta, 1992; Mazziotta et al., 1987; Minoshima et al., 1995; Ost te al., 2003; Reiman et al., 1989; Tjuvajev et al., 1999; Tyler & Byme, 1992; Vorstrup et al., 1986; Wackers, 1999; Yu et al., 2000]. For example a recent editorial in the New England Journal of Medicine emphasized the importance of PET in oncologic imaging [Koh, 2003].

The first step in PET is to inject the patient with a dose of a suitable radiopharmaceutical. For example in brain imaging a typical such radiopharmaceutical is flurodeoxyglucose (FDG), which is a normal molecule of glucose attached artificially to an atom of radioactive fluorine. The cells in the brain which are more active have a higher metabolism, need more energy, thus will absorb more FDG. The fluorine atom in the FDG molecule suffers a radioactive decay, emitting a positron. When a positron collides with an electron it liberates energy in the form of *two* beams of gamma rays travelling in *opposite* directions, which are picked by the PET scanner. SPECT is similar to PET but the radiopharmaceuticals decay to emit a *single* photon.

In both PET and SPECT the radiating sources are inside the body, and the aim is to determine the distribution $g(x_1, x_2)$ of the relevant radiopharmaceutical from measurements made outside the body of the emitted radiation. If $f(x_1, x_2)$ is the x–ray attenuation coefficient of the body, then it is straightforward to show that the intensity I outside the body measured by a detector which picks up only radiation along the straight line L is given by

$$I = \int_L \mathrm{e}^{-\int_{L(x)} f \mathrm{d}s} g \mathrm{d}\tau, \tag{1.1}$$

where τ is a parameter along L, and $L(x)$ denotes the section of L between the point (x_1, x_2) and the detector. The attenuation coefficient $f(x_1, x_2)$ is precisely the function measured by the usual computed tomography (CT). Thus the basic mathematical problem in SPECT is to determine the function $g(x_1, x_2)$ from the knowledge of the "transmission" function $f(x_1, x_2)$ (determined via CT) and the "emission" function I (known from the measurements).

In PET the situation is simpler. Indeed, since the sources eject particles *pairwise* in *opposite* directions and the radiation in opposite directions is measured *simultaneously*, Eq. (1.1) is replaced by

$$I = \int_L \mathrm{e}^{-\int_{L_+(x)} f \mathrm{d}s - \int_{L_-(x)} f \mathrm{d}s} g \mathrm{d}\tau, \tag{1.2}$$

where L_+, L_- are the two half–lines of L with endpoint x. Since $L_+ + L_- = L$, Eq. (1.2) becomes

$$I = \mathrm{e}^{-\int_L f \mathrm{d}\tau} \int_L g \mathrm{d}\tau.$$

Since both I and the integral of $f(x_1, x_2)$ are known (from the measurements of PET and of CT respectively), the basic mathematical problem of PET is to determine $g(x_1, x_2)$ from the knowledge of its line integrals. This mathematical problem is identical with the basic mathematical problem of CT.

In summary: In PET the main mathematical problem is to solve the equation

$$\int_L g \mathrm{d}\tau = I \mathrm{e}^{\int_L f \mathrm{d}\tau},$$

for $g(x_1, x_2)$ in terms of I and f. This problem is *identical* with the main mathematical problem of CT, thus there exist efficient numerical algorithm for its solution. In SPECT the main mathematical problem is to solve the Eq. (1.1) for $g(x_1, x_2)$ in terms of I and f.

For PET there exist two general approaches to reconstruction, one is based on the analytical inverse formula and the other is based on iterative techniques. Among the former approaches, filtered back projection (FBP) was until recently the most commonly used method of reconstruction in clinical practice. The approaches based on iterative techniques can be broadly divided in non–statistical techniques and statistical techniques [Lalush, 2004]. The latter techniques can be divided into two main groups, those that assume Gaussian noise and those that assume Poisson noise. For SPECT, until recently it was impossible to use analytical techniques. However, now that there exist an exact formula for the inversion it is possible to use analytical techniques. We have presented in Fokas et al. [2004b] a numerical implementation of the exact formula and have tested it on the realistic phantom of Garrity et al. [2003] with excellent results. The approach of filtered back projection is presented in Kunyansky [2001], and Natterer [2001]. Among the iterative techniques used for SPECT we mention the maximum likelihood (ML)–expected maximisation (EM) technique [Lange & Fessler, 1995; Miller et. al., 1985; Shepp & Vardi, 1982]. A significant improvement of this technique was presented in Green [1990], the so called one step late (OSL), where smoothing was added *without* making the iterative scheme prohibitively complicated. In clinical practice the most commonly used iterative technique [Hutton et. al., 1997] is the ordered subsets (OS)–EM [Hudson & Larkin, 1994] which uses different subsets of projections in each iteration (until all projections are used), and hence is much faster than ML–EM.

The paper is organized as follows: In Sec. 2 we review the main mathematical problem of MEG in the case of the spherical model. We present the exact formula expressing the part of the current that can be determined from the measurements, and we also give the exact formula for the minimizing current. Furthermore, we discuss how the mathematical data needed for the determination of the minimizing current can be obtained from the measurements. In Sec. 3 we present a novel derivation of the solution of the main mathematical problems of CT and PET, namely we derive the inverse Radon transform. This is done for two reasons: (a) for completeness and (b) because, a slight modification of this particular derivation of the inverse Radon transform, yields the inversion of Eq. (1.1). In Sec. 4 we present the solution of Eq. (1.1) and we also discuss the numerical implementation of this exact formula.

2 MEG

The current density $\mathbf{J}$ and the magnetic field $\mathbf{B}$ are related by the Maxwell equations. These equations can be simplified using two facts. First, the permeability of the tissue in the head denoted by μ is that of the free space, i.e. $\mu = \mu_0$. Second, the quasistatic approximation is valid, namely the terms $\partial\mathbf{E}/\partial t$ and $\partial\mathbf{B}/\partial t$ can be neglected, where $\mathbf{E}$ denotes the electric field. Using these facts the Maxwell equations become

$$\nabla \cdot \mathbf{B} = 0, \quad \nabla \wedge \mathbf{B} = \mu_0 \mathbf{J}, \tag{2.1}$$

where $\cdot$ and $\wedge$ denote the scalar and vector product, respectively, and ∇ denotes the usual gradient. Part of $\mathbf{J}$ is due to neuronal activity, and part of $\mathbf{J}$ is due to the electric field $\mathbf{E}$,

$$\mathbf{J} = \mathbf{J}^{\mathbf{p}} + \sigma \mathbf{E}, \tag{2.2}$$

where $\mathbf{J}^{\mathbf{p}}$ denotes the neuronal current (primary current) and σ denotes the conductivity. The electric field $\mathbf{E}$ satisfies $\nabla \wedge \mathbf{E} = \mathbf{0}$, thus there exists a scalar function V, called the voltage potential, such that

$$\mathbf{E} = -\nabla V. \tag{2.3}$$

Making the further assumption that $\sigma = \sigma_I$ inside the head and $\sigma = \sigma_O$ outside the head, where σ_O and σ_I are constants, Eqs. (2.1)–(2.3) imply the celebrated Geselowitz equation [Geselowitz, 1970]

$$\mathbf{B}(\mathbf{x}) = \frac{\mu_0}{4\pi}\int_\Omega \mathbf{J^p}(\mathbf{y}) \wedge \frac{\mathbf{x}-\mathbf{y}}{|\mathbf{x}-\mathbf{y}|^3}\mathrm{d}\mathbf{y} - \frac{\mu_0}{4\pi}(\sigma_I - \sigma_O)\int_{\partial\Omega} V(\mathbf{y})\mathbf{n}(\mathbf{y}) \wedge \frac{\mathbf{x}-\mathbf{y}}{|\mathbf{x}-\mathbf{y}|^3}\mathrm{d}S, \quad \mathbf{x} \notin \Omega, \tag{2.4}$$

where $|\mathbf{x}|$ denotes the length of the vector $\mathbf{x}$, Ω denotes the volume occupied by the head, $\partial\Omega$ is the boundary of Ω, $\mathbf{n}$ denotes the unit outward vector normal to the surface $\partial\Omega$, and $\mathrm{d}S$ denotes the infinitesimal surface element on $\partial\Omega$. For a recent rigorous derivation of this equation see Dassios & Kariotou [2003].

Equation (2.4) relates $\mathbf{J^p}$ inside the head with $\mathbf{B}$ outside the head. However, it also involves the value of V on the surface of the head. This serious complication can be avoided if one makes the simplifying assumption that the head is spherical. Then, Eq. (2.4) reduces to [Grynszpan & Geselowitz, 1973; Ilmoniemi et al., 1985; Sarvas, 1987]

$$\mathbf{B} = \mu_0 \nabla U, \qquad U(\mathbf{x}) = \frac{1}{4\pi}\int_{|\mathbf{y}|\le 1} \frac{\mathbf{J^p}(\mathbf{y}) \wedge \mathbf{y}\mathrm{d}\mathbf{y}}{|\mathbf{x}-\mathbf{y}|(|\mathbf{x}||\mathbf{x}-\mathbf{y}| + \mathbf{x}\cdot(\mathbf{x}-\mathbf{y}))} \cdot \mathbf{x}, \quad |\mathbf{x}| > 1. \tag{2.5}$$

2.1 Analytical results

The following basic theorem was derived in Fokas et al. [1996].

Theorem 2.1. The vector $\mathbf{J^p}(\mathbf{x})$ can be uniquely decomposed in the form

$$\mathbf{J^p}(\mathbf{x}) = J^\rho(\rho,\theta,\varphi)\mathbf{e}_\rho + J^\theta(\rho,\theta,\varphi)\mathbf{e}_\theta + J^\varphi(\rho,\theta,\varphi)\mathbf{e}_\varphi, \tag{2.6}$$

where $\mathbf{e}_\rho$, $\mathbf{e}_\theta$, $\mathbf{e}_\varphi$ are the unit vectors associated with the spherical coordinates $\rho > 0$, $0 \le \theta \le \pi$, $0 \le \varphi < 2\pi$, and the scalar functions J^θ and J^φ can be represented in the form

$$J^\theta = \frac{1}{\rho}\left(\frac{\partial G}{\partial\theta} - \frac{1}{\sin\theta}\frac{\partial F}{\partial\varphi}\right), \quad J^\varphi = \frac{1}{\rho}\left(\frac{1}{\sin\theta}\frac{\partial G}{\partial\varphi} + \frac{\partial F}{\partial\theta}\right), \tag{2.7}$$

where $G(\rho,\theta,\varphi)$ and $F(\rho,\theta,\varphi)$ are scalar functions of the arguments indicated.

Assume that $U(\mathbf{x})$ is defined in terms of $\mathbf{J^p}$ by Eq. (2.5). Then

$$U(\mathbf{x}) = -\frac{1}{4\pi}\int_{|\mathbf{y}|\leq 1}\frac{1}{|\mathbf{x}-\mathbf{y}|}\left(\frac{1}{|\mathbf{y}|^2}\int_{|\mathbf{y}|}^{1}\Delta_{\theta,\varphi}F(|\mathbf{z}|,\theta,\varphi)\mathrm{d}|\mathbf{z}|\right)\mathrm{d}\mathbf{y}, \quad |\mathbf{x}|>1, \tag{2.8}$$

where $\Delta_{\theta,\varphi}$ denotes the Laplacian with respect to the spherical coordinates θ and φ, i.e.

$$\Delta_{\theta,\varphi} = \frac{1}{\sin\theta}\left[\frac{\partial}{\partial\theta}\left(\sin\theta\frac{\partial}{\partial\theta}\right)+\frac{1}{\sin\theta}\frac{\partial^2}{\partial\varphi^2}\right].$$

Corollary (Non uniqueness of the inverse problem). Assume that $U(\mathbf{x})$ is defined in terms of $\mathbf{J^p}$ by Eq. (2.5). Let a vector $\mathbf{J^p}(\mathbf{x})$ be written in the form (2.6) where the scalar functions J^θ and J^φ are given in terms of the scalar function G and F by Eqs. (2.7).

The function $U(\mathbf{x})$ is *independent* of J^ρ and of G, and furthermore only certain moments of F can be computed in terms of U. In particular, $F(\rho,\theta,\varphi)$ is given by the expression

$$F(\rho,\theta,\varphi) = \sum_{\ell=1}^{\infty}\sum_{m=-\ell}^{\ell} f_{\ell,m}(\rho)Y_{\ell,m}(\theta,\varphi), \quad \rho<1, \quad 0\leq\theta\leq\pi, \quad 0\leq\varphi<2\pi,$$

where $Y_{\ell,m}$ are the usual spherical harmonics, the moments of $f_{\ell,m}(\rho)$ can be determined in terms of $c_{\ell,m}$,

$$\ell\int_0^1 \rho^{\ell+1}f_{\ell,m}(\rho)\mathrm{d}\rho = (2\ell+1)c_{\ell,m}, \tag{2.9}$$

and the constants $c_{\ell,m}$ can be determined from the given data using the fact that $U(\mathbf{x})$ can be expressed in the form

$$U(\rho,\theta,\varphi) = \sum_{\ell=1}^{\infty}\sum_{m=-\ell}^{\ell} c_{\ell,m}\rho^{-(\ell+1)}Y_{\ell,m}(\theta,\varphi), \quad \rho>1, \quad 0\leq\theta\leq\pi, \quad 0\leq\varphi\leq 2\pi. \tag{2.10}$$

Proof. Equation (2.8) implies

$$\begin{aligned} \Delta U &= \frac{1}{|\mathbf{x}|^2}\int_{|\mathbf{x}|}^{1}\Delta_{\theta,\varphi}F(|\mathbf{z}|,\theta,\varphi)\mathrm{d}|\mathbf{z}|, \quad |\mathbf{x}|<1, \\ \Delta U &= 0, \quad |\mathbf{x}|>1. \end{aligned} \tag{2.11}$$

Let us represent F and U in terms of spherical harmonics by

$$F(\rho,\theta,\varphi) = \sum_{\ell,m} f_{\ell,m}(\rho)Y_{\ell,m}(\theta,\varphi) \quad \text{and} \quad U(\rho,\theta,\varphi) = \sum_{\ell,m} u_{\ell,m}(\rho)Y_{\ell,m}(\theta,\varphi).$$

Then Eqs. (2.11) imply

$$u''_{\ell,m} + \frac{2}{\rho} u'_{\ell,m} - \frac{\ell(\ell+1)}{\rho^2} u_{\ell,m} = \begin{cases} -\frac{\ell(\ell+1)}{\rho^2} \int_\rho^1 f_{\ell,m}(\rho')\mathrm{d}\rho' & \rho < 1 \\ 0 & \rho > 1, \end{cases}$$

where prime denotes differentiation with respect to ρ. The general solution of the homogeneous problem is $\alpha\rho^\ell + \beta\rho^{-(\ell+1)}$, where α and β are constants and ℓ is a positive integer. Since $u_{\ell,m} \to 0$ as $\rho \to \infty$ it follows that

$$u_{\ell,m} = c_{\ell,m}\rho^{-(\ell+1)}.$$

To solve the inhomogeneous problem we use variation of parameters in the form $u_{\ell,m}(\rho) = A_{\ell,m}(\rho)\rho^\ell$. This implies

$$(A'_{\ell,m}\rho^{2\ell+2})' = -\ell(\ell+1)\alpha_{\ell,m}(\rho), \quad \alpha_{\ell,m}(\rho) \doteqdot \rho^\ell \int_\rho^1 f_{\ell,m}(\rho')\mathrm{d}\rho'.$$

Thus

$$A'_{\ell,m}\rho^{2\ell+2} = \ell(\ell+1)\int_\rho^1 \alpha_{\ell,m}(\rho')\mathrm{d}\rho' + A'_{\ell,m}(1).$$

Convergence at $\rho = 0$ implies

$$A'_{\ell,m}(1) + \ell(\ell+1)\int_0^1 \alpha_{\ell,m}(\rho')\mathrm{d}\rho' = 0. \tag{2.12}$$

Using $A_{\ell,m} = u_{\ell,m}\rho^{-\ell}$, we find

$$A'_{\ell,m}(1) = u'_{\ell,m}(1) - \ell u_{\ell,m}(1) = \left(c_{\ell,m}\rho^{-(\ell+1)}\right)'\Big|_{\rho=1} - \ell c_{\ell,m}\rho^{-(\ell+1)}\Big|_{\rho=1} = -(2\ell+1)c_{\ell,m}.$$

This equation together with (2.12) imply

$$\ell(\ell+1)\int_0^1 \alpha_{\ell,m}(\rho)\mathrm{d}\rho = (2\ell+1)c_{\ell,m}.$$

Using integration by parts we find (2.9). **QED**

Theorem 2.2. (Minimization of the energy norm). Define the energy by

$$W \doteqdot \int_{|\mathbf{x}|\le 1} |\mathbf{J}^\mathbf{p}|^2 \mathrm{d}\mathbf{x}. \tag{2.13}$$

Then if

$$\mathbf{J^p} = J^\rho \mathbf{e}_\rho + J^\theta \mathbf{e}_\theta + J^\varphi \mathbf{e}_\varphi,$$

where J^θ and J^φ are given by Eqs. (2.7), it follows that the minimum of W under the constrain

$$F = \sum_{\ell=1}^{\infty} \sum_{m=-\ell}^{\ell} f_{\ell,m}(\rho) Y_{\ell,m}(\theta,\varphi), \quad \ell \int_0^1 \rho^{\ell+1} f_{\ell,m}(\rho) \mathrm{d}\rho = (2\ell+1) c_{\ell,m},$$

where $Y_{\ell,m}$ are the usual spherical harmonics and $c_{\ell,m}$ are given constants, is achieved when

$$J^\rho = G = 0, \quad F = \sum_{\ell=1}^{\infty} \sum_{m=-\ell}^{\ell} \frac{(2\ell+1)(2\ell+3)}{\ell} c_{\ell,m} \rho^{\ell+1} Y_{\ell,m}(\theta,\varphi). \tag{2.14}$$

Proof. Substituting Eqs. (2.6) and (2.7) in the right–hand side of Eq. (2.13) we find

$$W = \int_{|\mathbf{x}|\leq 1} \left[(J^\rho)^2 + \frac{1}{\rho^2}\left(\frac{\partial G}{\partial \theta}\right)^2 + \frac{1}{\rho^2 \sin^2\theta}\left(\frac{\partial G}{\partial \varphi}\right)^2 + \frac{1}{\rho^2 \sin^2\theta}\left(\frac{\partial F}{\partial \varphi}\right)^2 + \frac{1}{\rho^2}\left(\frac{\partial F}{\partial \theta}\right)^2 \right] \mathrm{d}\mathbf{x},$$

where we have used that the term involving $G_\varphi F_\theta - G_\theta F_\varphi$ vanishes,

$$\int_0^1 \int_0^\pi \int_0^{2\pi} \frac{1}{\rho^2 \sin\theta} \left[-\frac{\partial G}{\partial \theta}\frac{\partial F}{\partial \varphi} + \frac{\partial G}{\partial \varphi}\frac{\partial F}{\partial \theta} \right] \rho^2 \sin\theta \mathrm{d}\rho \mathrm{d}\theta \mathrm{d}\varphi = 0.$$

The constraint involves only F, thus it follows that the minimal energy is achieved when $J^\rho = G = 0$ and when H is minimal, where

$$H = \int_0^1 \int_0^\pi \int_0^{2\pi} \left[\frac{1}{\rho^2 \sin^2\theta}\left(\frac{\partial F}{\partial \varphi}\right)^2 + \frac{1}{\rho^2}\left(\frac{\partial F}{\partial \theta}\right)^2 \right] \rho^2 \sin\theta \mathrm{d}\rho \mathrm{d}\theta \mathrm{d}\varphi. \tag{2.15}$$

The term inside the bracket equals $|\nabla F|^2 - (\frac{\partial F}{\partial \rho})^2$, which using integration by parts (with either F or $\frac{\partial F}{\partial \rho}$ equal to 0 at $|\mathbf{x}| = 1$), equals $-[F\Delta F + (\frac{\partial F}{\partial \rho})^2]$, where

$$\Delta F = \frac{\partial^2 F}{\partial \rho^2} + \frac{2}{\rho}\frac{\partial F}{\partial \rho} + \frac{1}{\rho^2}\Delta_{\theta,\varphi} F.$$

Using

$$F = \sum_{\ell,m} f_{\ell,m}(\rho) Y_{\ell,m}(\theta,\varphi), \quad \Delta_{\theta,\varphi} Y_{\ell,m} = -\ell(\ell+1) Y_{\ell,m},$$

and the orthogonality of the spherical harmonics, it follows that

$$H = -\sum_{\ell,m} \int_0^1 \left\{ \left[f''_{\ell,m}(\rho) + \frac{2}{\rho} f'_{\ell,m}(\rho) - \frac{\ell(\ell+1)}{\rho^2} f_{\ell,m}(\rho) \right] f_{\ell,m}(\rho) + (f'_{\ell,m}(\rho))^2 \right\} \rho^2 \mathrm{d}\rho.$$

Hence,

$$H = -\sum_{\ell,m} \left[\int_0^1 \left\{ (f_{\ell,m} f'_{\ell,m} \rho^2)' - \ell(\ell+1) f^2_{\ell,m}(\rho) \right\} \mathrm{d}\rho \right].$$

Thus, provided that either $f_{\ell,m}(1)$ or $f'_{\ell,m}(1)$ equals zero, we find

$$H = \sum_{\ell,m} \ell(\ell+1) \int_0^1 f^2_{\ell,m}(\rho) \mathrm{d}\rho.$$

The assumption that $f_{\ell,m}(1) = 0$ is without loss of generality since the tangential part of the energy which is given by Eq. (2.15) does not involve differentiation over ρ, thus in general (2.15) can be obtained by approximating f by functions equal to zero at $\rho = 1$ and then passing to the limit.

The minimization of this H, under the constraint (2.9), implies (2.14).

We note that Eq. (2.5) implies that $U(\mathbf{x})$ behaves like $\mathrm{O}(\rho^{-2})$, hence $\ell > 0$ in Eq. (2.10), $c_{00} = 0$, and the sum (2.14) starts with $\ell = 1$. **QED**

2.2 Determination of $c_{\ell,m}$ from the measurements

In Eq. (2.10), $Y_{\ell,m}$ denotes the spherical harmonics, namely

$$\begin{aligned} Y_{\ell,m}(\theta,\varphi) &= a_{\ell,m} P_{\ell,m}(\cos\theta) \mathrm{e}^{im\varphi}, \\ Y_{\ell,-m} &= (-1)^m \overline{Y_{\ell,m}}, \qquad \ell \geq 1, \quad 0 \leq m \leq \ell, \end{aligned} \tag{2.16}$$

where the bar denotes complex conjugate and

$$a_{\ell,m} = \sqrt{\frac{2\ell+1}{4\pi} \frac{(\ell-m)!}{(\ell+m)!}}.$$

$P_{\ell,m}$ are the Legendre functions, namely

$$P_{\ell,m}(x) = (-1)^m (1-x^2)^{m/2} \frac{\mathrm{d}^m}{\mathrm{d}x^m} P_\ell(x),$$

where

$$P_\ell(x) = \frac{1}{2^\ell \ell!} \frac{\mathrm{d}^\ell}{\mathrm{d}x^\ell} (x^2-1)^\ell$$

are the usual Legendre polynomials of degree ℓ.

The SQUID measures the component $|\mathbf{B}'|$ of the magnetic field $\mathbf{B}$ along the axis of measurements specified by the unit vector $\mathbf{l} = (a, b, c)$. Since $\mathbf{B} \cdot \mathbf{l} = |\mathbf{B}'|$ and $\mathbf{B} = \mu_0 \nabla U$ we obtain

$$aU_x + bU_y + cU_z = \frac{|\mathbf{B}'|}{\mu_0} = \gamma.$$

Writing this equation in spherical coordinates we find

$$AU_\rho + BU_\theta + CU_\varphi = \gamma, \tag{2.17}$$

where

$$A = a \sin\theta \cos\varphi + b \sin\theta \sin\varphi + c \cos\theta,$$

$$B = \frac{1}{\rho}(a \cos\theta \cos\varphi + b \cos\theta \sin\varphi - c \sin\theta),$$

$$C = -\frac{1}{\rho \sin\theta}(a \sin\varphi - b \cos\varphi).$$

Equation (2.10), i.e. equation

$$U = \sum_{\ell=1}^{\infty} \rho^{-(\ell+1)} \sum_{m=-\ell}^{\ell} c_{\ell,m} Y_{\ell,m}(\theta, \varphi), \tag{2.18}$$

involves the following sum denoted by Σ,

$$\Sigma = c_{\ell,0} Y_{\ell,0} + \sum_{m=1}^{\ell} c_{\ell,m} Y_{\ell,m} + \sum_{m=-\ell}^{-1} c_{\ell,m} Y_{\ell,m}. \tag{2.19}$$

Using the second of Eqs. (2.16), as well as the relation

$$c_{\ell,-m} = (-1)^m \overline{c_{\ell,m}}, \tag{2.20}$$

Eq. (2.19) becomes

$$\Sigma = c_{\ell,0} Y_{\ell,0} + \sum_{m=1}^{\ell} c_{\ell,m} Y_{\ell,m} + \sum_{m=1}^{\ell} \overline{c_{\ell,m}}\, \overline{Y_{\ell,m}}.$$

Thus

$$\Sigma = c_{\ell,0} a_{\ell,0} P_{\ell,0}(\cos\theta) + \sum_{m=1}^{\ell} c_{\ell,m} a_{\ell,m} P_{\ell,m}(\cos\theta) \mathrm{e}^{\mathrm{i}m\varphi} + \sum_{m=1}^{\ell} \overline{c_{\ell,m}} a_{\ell,m} P_{\ell,m}(\cos\theta) \mathrm{e}^{-\mathrm{i}m\varphi}. \tag{2.21}$$

Denoting $c_{\ell,m} = c_{\ell,m}^{Re} + \mathrm{i} c_{\ell,m}^{Im}$ and using the fact that the quantities $c_{\ell,m}\mathrm{e}^{\mathrm{i}m\varphi}$ and $\overline{c_{\ell,m}}\mathrm{e}^{-\mathrm{i}m\varphi}$ have the same real part, which equals

$$c_{\ell,m}^{Re} \cos m\varphi - c_{\ell,m}^{Im} \sin m\varphi,$$

Eqs. (2.18) and (2.21) yield

$$U = \sum_{\ell=1}^{\infty} \rho^{-(\ell+1)} \left[c_{\ell,0}^{Re} a_{\ell,0} P_{\ell,0}(\cos\theta) + 2 \sum_{m=1}^{\ell} \left(c_{\ell,m}^{Re} \cos m\varphi - c_{\ell,m}^{Im} \sin m\varphi \right) a_{\ell,m} P_{\ell,m}(\cos\theta) \right].$$

Using this equation to calculate the derivatives of U with respect to ρ, θ, φ, and then substituting the resulting equations into Eq. (2.17) we find an equation coupling the given data γ with the constants $c_{\ell,m}^{Re}$ and $c_{\ell,m}^{Im}$.

Since we can only have simultaneous measurements in 248 different points, relation (2.17) gives a highly underdetermined system with 248 equations for the calculation of the coefficients $c_{\ell,m}^{Re}$ and $c_{\ell,m}^{Im}$. If we choose an upper cutoff ℓ_{max}, then it follows that Eq. (2.17) involves $\ell_{max}(\ell_{max}+2)$ constants $c_{\ell,m}$. Thus we choose ℓ_{max} such that $\ell_{max}(\ell_{max}+2) < 248$ and then calculate the constants $c_{\ell,m}$ using the least–square method, i.e. if $A_i = B_i$ are the 248 equations, the quantity

$$(A_1 - B_1)^2 + (A_2 - B_2)^2 + \ldots + (A_{248} - B_{248})^2$$

is minimum. This can be done by using standard subroutines. We use subroutine `dlsbrr` [Digital Equipment Corporation, 1998].

2.3 Computation of the minimizing current

Using relations (2.14), (2.16) and (2.20), the real parts of the functions J^θ, J^φ defined in (2.7) (with $G=0$) are given by

$$J^\theta(\rho,\theta,\varphi) = \frac{2}{\sin\theta} \sum_{\ell=1}^{\ell_{max}} \frac{(2\ell+1)(2\ell+3)}{\ell} \rho^\ell \cdot \left(\sum_{m=1}^{\ell} m (c_{\ell,m}^{Re} \sin m\varphi + c_{\ell,m}^{Im} \cos m\varphi) a_{\ell,m} P_{\ell,m}(\cos\theta) \right), \tag{2.22}$$

and

$$J^\varphi(\rho,\theta,\varphi) = -\sin\theta \sum_{\ell=1}^{\ell_{max}} \frac{(2\ell+1)(2\ell+3)}{\ell} \rho^\ell \cdot \left(c_{\ell,0}^{Re} a_{\ell,0} P'_{\ell,0}(\cos\theta) + 2 \sum_{m=1}^{\ell} (c_{\ell,m}^{Re} \cos m\varphi - c_{\ell,m}^{Im} \sin m\varphi) a_{\ell,m} P'_{\ell,m}(\cos\theta) \right). \tag{2.23}$$

Recall that the Legendre functions satisfy the recurrence relation

$$P'_{\ell,m}(x) = -\frac{mx}{1-x^2}P_{\ell,m}(x) - \frac{1}{\sqrt{1-x^2}}P_{\ell,m+1}(x).$$

Therefore

$$\begin{aligned}
-\sin\theta P'_{\ell,0}(\cos\theta) &= P_{\ell,1}(\cos\theta), \quad \text{for} \quad m=0,\\
-\sin\theta P'_{\ell,m}(\cos\theta) &= \frac{m\cos\theta}{\sin\theta}P_{\ell,m}(\cos\theta) + P_{\ell,m+1}(\cos\theta), \quad \text{for} \quad m>0.
\end{aligned} \tag{2.24}$$

In order to calculate numerically the current we apply the following procedure: We first calculate the Legendre functions $P_{\ell,m}(\cos\theta)$, using subroutine `plgndr` from Numerical Recipes [Press et al., 1992]. In a separate subroutine we calculate the quantities $P_{\ell,m}(\cos\theta)/\sin\theta$ (for this purpose we have developed a subroutine similar to `plgndr`). These quantities appear in both (2.22) and in the second relation of (2.24). Note that these quantities are valid even for $\theta = 0$ and $\theta = \pi$. We then calculate the quantities $-\sin\theta P'_{\ell,m}(\cos\theta)$ using Eq. (2.24). Finally, we take a value of ρ such as $0 < \rho < 1$ and calculate $J^\theta(\rho,\theta,\varphi)$ using (2.22), and $J^\varphi(\rho,\theta,\varphi)$ using (2.23).

In Fig. 1 we present the density plots of the minimizing current $(J^\theta)^2 + (J^\varphi)^2$ in various cuts perpendicular to the z–axis. The real data used were provided from the Department of Neurosurgery, University of Texas Medical School. These density plots were drawn by using `Mathematica` [Wolfram, 1999]. The dark color represents zero values while the white color represents the maximum value of the constructed function. The value of ℓ_{max} is 10 and the construction is taking place in a 200×200 grid.

3 The Mathematics of CT and of PET

It was shown in the introduction that the basic mathematical problem of both CT and PET is the determination of a function from its line integral. The line integral of a function is called its *Radon transform.* Thus, the main mathematical problem of both CT and PET is the derivation

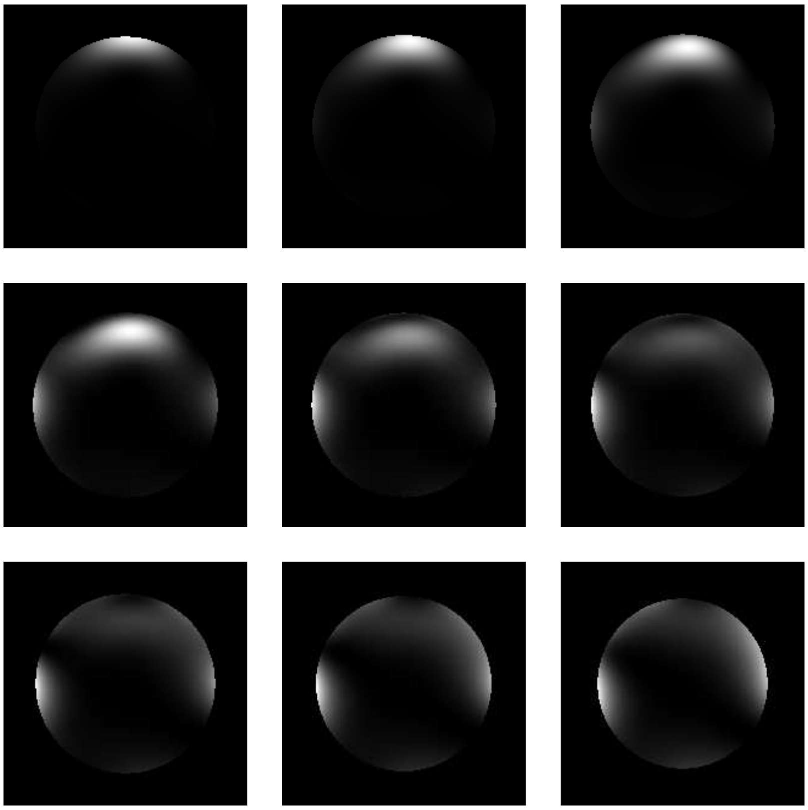

Figure 1: Density plots for the minimizing current with real data. Starting from top left, the values at the z–axis are -0.18, -0.12, -0.06, 0, 0.06, 0.12, 0.18, 0.24, and 0.30.

of the *inverse Radon transform*. For this purpose we first introduce some notations: A line L can be specified by the angle θ it makes with the x_1 axis and its distance ρ from the origin, see Fig. 2. Let $\mathbf{k}$ and $\mathbf{k}^{\perp}$ denote two unit vectors parallel and perpendicular to line L, respectively. Then

$$\mathbf{x} = \tau\mathbf{k} + \rho\mathbf{k}^{\perp},$$

or

$$(x_1, x_2) = \tau(\cos\theta, \sin\theta) + \rho(-\sin\theta, \cos\theta).$$

Hence

$$x_1 = \tau\cos\theta - \rho\sin\theta, \quad x_2 = \tau\sin\theta + \rho\cos\theta, \tag{3.1}$$

and the inverse of this transformation is

$$\tau = x_2 \sin\theta + x_1 \cos\theta, \quad \rho = x_2 \cos\theta - x_1 \sin\theta. \tag{3.2}$$

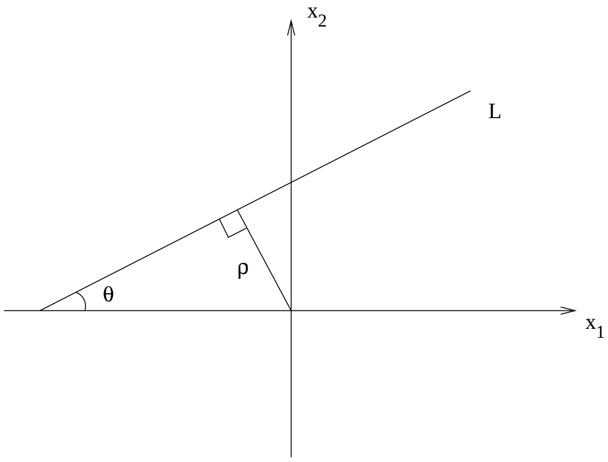

Figure 2: Local coordinates for the mathematical formulation of CT and PET.

A function $f(x_1, x_2)$ rewritten in the local coordinates τ, ρ, θ will be denoted by $F_\theta(\tau, \rho)$,

$$F_\theta(\tau, \rho) = f(\tau\cos\theta - \rho\sin\theta, \tau\sin\theta + \rho\cos\theta). \tag{3.3}$$

The Radon transform of a function f will be denoted by $\hat{f}$. In order to compute $\hat{f}$, we first write f in local coordinates and then integrate with respect to τ,

$$\hat{f}(\rho, \theta) = \int_{-\infty}^{\infty} F_\theta(\tau, \rho)\mathrm{d}\tau. \tag{3.4}$$

Theorem 3.1. Let the Radon transform of a function $f(x_1, x_2)$ be defined by Eq. (3.4), where it is assumed that $f(x_1, x_2)$ decays sufficiently fast as $|x_1| + |x_2| \to \infty$. Then the inverse Radon transform is given by

$$f(x_1, x_2) = \frac{1}{4\mathrm{i}\pi^2}(\partial_{x_1} - \mathrm{i}\partial_{x_2}) \int_0^{2\pi} \mathrm{e}^{\mathrm{i}\theta} \left(\oint_{-\infty}^{\infty} \frac{\hat{f}(\rho, \theta)\mathrm{d}\rho}{\rho - (x_2\cos\theta - x_1\sin\theta)} \right) \mathrm{d}\theta. \tag{3.5}$$

Proof. Let the scalar function $\mu(x_1, x_2, \lambda)$, $x_1 \in \mathbb{R}$, $x_2 \in \mathbb{R}$, $\lambda \in \mathbb{C}$, $|\lambda| \neq 1$, satisfy

$$\left(\frac{1}{2}\left(\lambda + \frac{1}{\lambda}\right)\partial_{x_1} + \frac{1}{2\mathrm{i}}\left(\lambda - \frac{1}{\lambda}\right)\partial_{x_2} \right) \mu(x_1, x_2, \lambda) = f(x_1, x_2). \tag{3.6}$$

Define the complex variable z by

$$z = \frac{1}{2\mathrm{i}}\left(\lambda - \frac{1}{\lambda}\right)x_1 - \frac{1}{2}\left(\lambda + \frac{1}{\lambda}\right)x_2. \tag{3.7}$$

The complex conjugate of Eq. (3.7) is

$$\bar{z} = -\frac{1}{2\mathrm{i}}\left(\bar{\lambda} - \frac{1}{\bar{\lambda}}\right)x_1 - \frac{1}{2}\left(\bar{\lambda} + \frac{1}{\bar{\lambda}}\right)x_2. \tag{3.8}$$

Equations (3.7) and (3.8) define a change of variables from (x_1, x_2) to $(z, \bar{z})$:

$$\partial_{x_1} = \frac{1}{2\mathrm{i}}\left(\lambda - \frac{1}{\lambda}\right)\partial_z - \frac{1}{2\mathrm{i}}\left(\bar{\lambda} + \frac{1}{\bar{\lambda}}\right)\partial_{\bar{z}}, \quad \partial_{x_2} = -\frac{1}{2}\left(\lambda - \frac{1}{\lambda}\right)\partial_z - \frac{1}{2}\left(\bar{\lambda} + \frac{1}{\bar{\lambda}}\right)\partial_{\bar{z}}.$$

Hence Eq. (3.6) becomes

$$\nu(|\lambda|)\frac{\partial\mu}{\partial\bar{z}} = f(x_1, x_2), \quad |\lambda| \neq 1, \quad (x_1, x_2) \in \mathbb{R}^2, \quad \nu(|\lambda|) = \frac{1}{2\mathrm{i}}\left(\frac{1}{|\lambda|^2} - |\lambda|^2\right).$$

We supplement this equation with the boundary condition

$$\mu = \mathrm{O}\left(\frac{1}{z}\right), \quad z \to \infty.$$

The solution of this equation is

$$\mu(x_1, x_2) = -\frac{1}{\pi}\int\int \frac{f}{\nu(|\lambda|)}\frac{\mathrm{d}z'_R\mathrm{d}z'_I}{z' - z}.$$

Using $\mathrm{d}z_R\mathrm{d}z_I = |\nu(|\lambda|)|\mathrm{d}x_1\mathrm{d}x_2$ the above equation yields

$$\mu(x_1, x_2, \lambda) = \frac{1}{2\pi\mathrm{i}}\mathrm{sgn}\left(\frac{1}{|\lambda|^2} - |\lambda|^2\right)\iint_{\mathbb{R}^2} \frac{f(x'_1, x'_2)}{z' - z}\mathrm{d}x'_1\mathrm{d}x'_2, \quad |\lambda| \neq 1. \tag{3.9}$$

Since the only dependence of μ on λ is via z and z', it follows that μ is an analytic function of λ. Also, it can be shown that $\mu = \mathrm{O}(1/\lambda)$ as $\lambda \to \infty$. Thus μ can be uniquely reconstructed if we take its "jump" across the unit circle:

$$\begin{aligned} \mu(x_1, x_2, \lambda) &= \frac{1}{2\pi}\int_0^{2\pi} \frac{J(x_1, x_2, \theta')\mathrm{e}^{\mathrm{i}\theta'}}{\mathrm{e}^{\mathrm{i}\theta'} - \lambda}\mathrm{d}\theta', \\ J(x_1, x_2, \theta) &= \mu(x_1, x_2, \lambda^+) - \mu(x_1, x_2, \lambda^-), \end{aligned} \tag{3.10}$$

where

$$\lambda^\pm = (1 \mp \varepsilon)\mathrm{e}^{\mathrm{i}\theta}, \quad \varepsilon \to 0, \quad \varepsilon > 0, \quad 0 \leq \theta \leq \pi. \tag{3.11}$$

It is shown in the Appendix that

$$\mu(x_1,x_2,\lambda^{\pm}) = \mp P^{\mp}\hat{f}(\rho,\theta) - \int_{\tau}^{\infty} F_\theta(\tau',\rho)\mathrm{d}\tau', \tag{3.12}$$

where $P^{\pm}$ denote the usual projection operators in the variable ρ, i.e.

$$(P^{\pm}g)(\rho) = \lim_{\substack{\varepsilon\to 0\\ \varepsilon>0}} \frac{1}{2\pi\mathrm{i}}\int_{-\infty}^{\infty}\frac{g(\rho')\mathrm{d}\rho'}{\rho'-(\rho\pm\mathrm{i}\varepsilon)} = \pm\frac{g(\rho)}{2} + \frac{1}{2\pi\mathrm{i}}\oint_{-\infty}^{\infty}\frac{g(\rho')\mathrm{d}\rho'}{\rho'-\rho}, \tag{3.13}$$

and $\oint$ denotes the principal value integral. Hence Eqs. (3.10) imply

$$J(x_1,x_2,\theta) = -\frac{1}{\pi\mathrm{i}}\oint_{-\infty}^{\infty}\frac{\hat{f}(\rho',\theta)\mathrm{d}\rho'}{\rho'-\rho}. \tag{3.14}$$

Equation (3.12) implies

$$\mu(x_1,x_2,\lambda) = -\frac{1}{2\pi}\left(\int_0^{2\pi} J(x_1,x_2,\theta)\mathrm{e}^{\mathrm{i}\theta}\mathrm{d}\theta\right)\frac{1}{\lambda} + \mathrm{O}\left(\frac{1}{\lambda^2}\right).$$

Substituting this expression in Eq. (3.6) we find

$$f(x_1,x_2) = \frac{1}{2}(\partial_{x_1} - \mathrm{i}\partial_{x_2})\left(-\frac{1}{2\pi}\int_0^{2\pi} J(x_1,x_2,\theta)\mathrm{e}^{\mathrm{i}\theta}\mathrm{d}\theta\right). \tag{3.15}$$

Replacing in this equation J by the right–hand side of Eq. (3.14) we find Eq. (3.5). **QED**

4 SPECT

The line integral of the function g with respect to the weight f appearing in Eq. (1.1) is called the *attenuated Radon transform* of g (with the attenuation specified by f) and will be denoted by $\hat{g}_f$. In order to compute $\hat{g}_f$, we write both g and f in local coordinates and then evaluate the following integral

$$\hat{g}_f(\rho,\theta) = \int_{-\infty}^{\infty} \mathrm{e}^{-\int_\tau^\infty F_\theta(s,\rho)\mathrm{d}s} G_\theta(\tau,\rho)\mathrm{d}\tau. \tag{4.1}$$

4.1 Analytical results

Theorem 4.1. Let the *attenuated Radon transform* of function $g(x_1,x_2)$ with the attenuation $f(x_1,x_2)$ be given by (4.1), where it is assumed that both functions f and g decay sufficiently fast as $|x_1|+|x_2|\to\infty$. Then the inverse attenuated Radon transform is given by

$$g(x_1,x_2)=-\frac{1}{4\pi}(\partial_{x_1}-\mathrm{i}\partial_{x_2})\int_0^{2\pi}J(x_1,x_2,\theta)\mathrm{e}^{\mathrm{i}\theta}\mathrm{d}\theta, \tag{4.2}$$

where J is defined by

$$J(x_1,x_2,\theta)=-\mathrm{e}^{\int_\tau^\infty F_\theta(\tau',\rho)\mathrm{d}\tau'}\left(\mathrm{e}^{P^-\hat{f}(\rho,\theta)}P^-\mathrm{e}^{-P^-\hat{f}(\rho,\theta)}+\mathrm{e}^{-P^+\hat{f}(\rho,\theta)}P^+\mathrm{e}^{P^+\hat{f}(\rho,\theta)}\right)\hat{g}_f(\rho,\theta), \tag{4.3}$$

$F_\theta(\tau,\rho)$ is defined in terms of f by Eq. (3.3), $\hat{f}(\rho,\theta)$ denotes the Radon transform of f, and the projection operators $P^\pm$ are defined by Eqs. (3.13).

Proof. Let $\mu(x_1,x_2,\lambda)$ satisfy the equation

$$\left(\frac{1}{2}\left(\lambda+\frac{1}{\lambda}\right)\partial_{x_1}+\frac{1}{2\mathrm{i}}\left(\lambda-\frac{1}{\lambda}\right)\partial_{x_2}+f(x_1,x_2)\right)\mu(x_1,x_2,\lambda)=g(x_1,x_2).$$

This equation can be rewritten as

$$\frac{\partial\mu}{\partial\bar{z}}+\frac{f}{\nu}\mu=\frac{g}{\nu}.$$

Hence

$$\frac{\partial}{\partial\bar{z}}\left(\mu\exp\left[\partial_{\bar{z}}^{-1}\left(\frac{f}{\nu}\right)\right]\right)=\frac{g}{\nu}\exp\left[\partial_{\bar{z}}^{-1}\left(\frac{f}{\nu}\right)\right],$$

or

$$\mu\exp\left[\partial_{\bar{z}}^{-1}\left(\frac{f}{\nu}\right)\right]=\partial_{\bar{z}}^{-1}\left(\frac{g}{\nu}\exp\left[\partial_{\bar{z}}^{-1}\left(\frac{f}{\nu}\right)\right]\right). \tag{4.4}$$

Equation (3.12) can be written as

$$\lim_{\lambda\to\lambda^\pm}\left\{\partial_{\bar{z}}^{-1}\left(\frac{f(x_1,x_2)}{\nu(\lambda)}\right)\right\}=\mp P^\mp\hat{f}(\rho,\theta)-\int_\tau^\infty F_\theta(\tau',\rho)\mathrm{d}\tau'. \tag{4.5}$$

Thus, we can compute the limit of Eq. (4.4) as $\lambda\to\lambda^\pm$. Indeed, replacing in this equation $\partial_{\bar{z}}^{-1}\left(\frac{f}{\nu}\right)$ by the right–hand side of Eq. (4.5) we find

$$\mu(x_1,x_2,\lambda^\pm)\mathrm{e}^{\mp P^\mp\hat{f}(\rho,\theta)}\mathrm{e}^{-\int_\tau^\infty F_\theta(\tau',\rho)\mathrm{d}\tau'}=\partial_{\bar{z}}^{-1}\left(\frac{g(x_1,x_2)}{\nu(\lambda)}\mathrm{e}^{\mp P^\mp\hat{f}(\rho,\theta)}\mathrm{e}^{-\int_\tau^\infty F_\theta(\tau',\rho)\mathrm{d}\tau'}\right).$$

For the computation of the right–hand side of this equation we use again Eq. (4.5), where f is replaced by g times the two exponentials appearing in the above relation. Hence

$$\mu(x_1, x_2, \lambda^{\pm}) \mathrm{e}^{\mp P^{\mp} \hat{f}(\rho,\theta)} \mathrm{e}^{-\int_\tau^\infty F_\theta(\tau',\rho)\mathrm{d}\tau'} =$$

$$\mp P^{\mp} \mathrm{e}^{\mp P^{\mp} \hat{f}(\rho,\theta)} \hat{g}_f(\rho,\theta) - \int_\tau^\infty G_\theta(\tau'\rho) \mathrm{e}^{\mp P^{\mp} \hat{f}(\rho,\theta)} \mathrm{e}^{-\int_{\tau'}^\infty F_\theta(s,\rho)\mathrm{d}s} \mathrm{d}\tau'. \tag{4.6}$$

Note that the term $\exp[\mp P^{\mp} \hat{f}]$ is independent of τ', thus this term comes out of the integral $\int_\tau^\infty$, and furthermore the same term appears in the left–hand side of Eq. (4.6). Hence when computing the jump $\mu(x_1, x_2, \lambda^+) - \mu(x_1, x_2, \lambda^-)$, the second term in the right–hand side of Eq. (4.6) cancels and we find that the relevant jump in now given by Eq. (4.3), where τ and ρ are expressed in terms of x_1 and x_2 by Eqs. (3.2).

The first of Eqs. (3.10) is still valid, furthermore Eq. (3.15) is valid if f is replaced by g. Hence replacing in Eq. (3.15) f by g we find (4.2). This formula is equivalent to Novikov's formula [Novikov, 2002]. **QED**

4.2 Numerical implementation

4.2.1 CT

Taking the real part of Eq. (3.5) it follows that $f(x_1, x_2)$ is given by

$$f(x_1, x_2) = -\frac{1}{4\pi^2} \int_0^{2\pi} h_\rho(\rho,\theta)\mathrm{d}\theta, \tag{4.7}$$

where $h(\rho,\theta)$ is defined by equation

$$h(\rho,\theta) = \oint_{-\infty}^{\infty} \frac{\hat{f}(\rho',\theta)}{\rho' - \rho} \mathrm{d}\rho', \tag{4.8}$$

and ρ is given by the second of Eqs. (3.2).

We assume that $f(x_1, x_2)$ has compact support, namely $f(x_1, x_2) = 0$, for ${x_1}^2 + {x_2}^2 \geq 1$. For the numerical calculation of the integral in (4.7) we use the formula

$$\int_0^{2\pi} g(\theta)\mathrm{d}\theta = \frac{2\pi}{N} \sum_{i=0}^{N-1} g\left(\frac{2\pi i}{N}\right). \tag{4.9}$$

Since g is analytic and periodic, this equispaced quadrature converges at spectral speed [Fornberg, 1996]. In other words, (4.9) represents the optimal quadrature formula for the above integral and its implementation is likely to result in high precision even for relatively small values of N. For the numerical calculation of $h_\rho(\rho,\theta)$ we suppose that $\hat{f}(\rho,\theta)$ is given, for every θ, at n equally spaced points $\rho_i \in [-1,1]$, i.e. we suppose that $\hat{f}_i = \hat{f}(\rho_i,\theta)$ are known. Moreover, in each interval $[\rho_i, \rho_{i+1}]$ we approximate $\hat{f}(\rho,\theta)$ using the relation

$$\hat{f}(\rho,\theta) = S_i(\rho,\theta) = A_i\hat{f}_i + B_i\hat{f}_{i+1} + C_i\hat{f}_i'' + D_i\hat{f}_{i+1}'', \tag{4.10}$$

where

$$A_i = \frac{\rho_{i+1}-\rho}{\rho_{i+1}-\rho_i}, \quad B_i = 1 - A_i, \quad C_i = \frac{1}{6}({A_i}^3 - A_i)(\rho_{i+1}-\rho_i)^2, \quad D_i = \frac{1}{6}({B_i}^3 - B_i)(\rho_{i+1}-\rho_i)^2,$$

and $\hat{f}_i''$ denotes the second derivative of $\hat{f}(\rho,\theta)$ with respect to ρ, at $\rho = \rho_i$. In other words, we approximate $\hat{f}(\rho,\theta)$ by a cubic spline (in ρ) with equally–spaced nodes. Integrating the spline, we derive a well–known quadrature formula which, in our setting, reads

$$h(\rho,\theta) = \sum_{i=1}^{n-1}\int_{\rho_i}^{\rho_{i+1}} \frac{S_i(\rho',\theta)}{\rho'-\rho}\mathrm{d}\rho'.$$

Following straightforward calculations we obtain

$$\begin{aligned} h_\rho(\rho,\theta) &= \sum_{i=1}^{n-1}\left\{ \frac{\hat{f}_i}{\rho_i-\rho} - \frac{\hat{f}_{i+1}}{\rho_{i+1}-\rho} - \frac{1}{4}(\rho_i - 3\rho_{i+1} + 2\rho)\hat{f}_i'' - \frac{1}{4}(3\rho_i - \rho_{i+1} - 2\rho)\hat{f}_{i+1}'' \right. \\ &+ \left[\frac{\hat{f}_i - \hat{f}_{i+1}}{\rho_i - \rho_{i+1}} - \frac{1}{6}\left(\rho_i - \rho_{i+1} - \frac{3(\rho_{i+1}-\rho)^2}{\rho_i-\rho_{i+1}}\right)\hat{f}_i'' \right. \\ &+ \left.\left. \frac{1}{6}\left(\rho_i - \rho_{i+1} - \frac{3(\rho_i-\rho)^2}{\rho_i-\rho_{i+1}}\right)\hat{f}_{i+1}''\right] \ln\left|\frac{\rho_{i+1}-\rho}{\rho_i-\rho}\right| \right\}. \end{aligned} \tag{4.11}$$

In order to calculate numerically $f(x_1,x_2)$ from the data $\hat{f}(\rho,\theta)$ we first compute the second derivatives $\hat{f}_i''$. For this purpose we use the subroutine `spline` from Numerical Recipes [Press et al., 1992], setting $\hat{f}_1'' = \hat{f}_n'' = 0$ (i.e. we use the natural cubic spline interpolation). Then, for any x_1 and x_2, we calculate (for any θ) ρ using the second of Eqs. (3.2) and $h_\rho(\rho,\theta)$ using (4.11). Finally we calculate $f(x_1,x_2)$ using (4.7).

We note that (4.11) contains the term

$$\ln\left|\frac{\rho_{i+1}-\rho}{\rho_i-\rho}\right|.$$

However, since for the reconstruction the number of the points for x_1 and x_2 can be different than the number of the ρ points, in general $\rho \neq \rho_{i+1}$ and $\rho \neq \rho_i$.

4.2.2 SPECT

We denote the first exponential term of the right–hand side of (4.3) by $I(\tau,\rho,\theta)$, i.e.

$$I(\tau,\rho,\theta) = \exp\left[\int_{\tau}^{\sqrt{1-\rho^2}} F_\theta(\tau',\rho)\mathrm{d}\tau'\right]. \tag{4.12}$$

Note that, since we have assumed compact support, the integration domain is finite, i.e. $[\tau, \sqrt{1-\rho^2}]$, and $F_\theta(\tau,\rho)=0$ for $|\rho|\geq 1$, or for $|\tau|\geq\sqrt{1-\rho^2}$.

The definitions (3.13) become

$$P^{\pm}\hat{f}(\rho,\theta) = \pm\frac{1}{2}\hat{f}(\rho,\theta) - \frac{\mathrm{i}}{2\pi}h(\rho,\theta).$$

Moreover

$$\begin{aligned}
\exp\left[P^{\pm}\hat{f}(\rho,\theta)\right] &= \exp\left[\pm\frac{1}{2}\hat{f}(\rho,\theta)\right]\left(\cos\frac{h(\rho,\theta)}{2\pi} - \mathrm{i}\sin\frac{h(\rho,\theta)}{2\pi}\right),\\
\exp\left[-P^{\pm}\hat{f}(\rho,\theta)\right] &= \exp\left[\mp\frac{1}{2}\hat{f}(\rho,\theta)\right]\left(\cos\frac{h(\rho,\theta)}{2\pi} + \mathrm{i}\sin\frac{h(\rho,\theta)}{2\pi}\right).
\end{aligned}$$

We introduce the following notation:

$$f^{cpe}(\rho,\theta) = \mathrm{e}^{\frac{1}{2}\hat{f}(\rho,\theta)}\cos\frac{h(\rho,\theta)}{2\pi}, \quad f^{spe}(\rho,\theta) = \mathrm{e}^{\frac{1}{2}\hat{f}(\rho,\theta)}\sin\frac{h(\rho,\theta)}{2\pi}, \tag{4.13}$$

$$f^{cme}(\rho,\theta) = \mathrm{e}^{-\frac{1}{2}\hat{f}(\rho,\theta)}\cos\frac{h(\rho,\theta)}{2\pi}, \quad f^{sme}(\rho,\theta) = \mathrm{e}^{-\frac{1}{2}\hat{f}(\rho,\theta)}\sin\frac{h(\rho,\theta)}{2\pi}, \tag{4.14}$$

$$f^{c}(\rho,\theta) = f^{cpe}(\rho,\theta)\hat{g}_f(\rho,\theta), \quad f^{s}(\rho,\theta) = f^{spe}(\rho,\theta)\hat{g}_f(\rho,\theta). \tag{4.15}$$

Using this notation and setting $R(\tau,\rho,\theta) = -J(\tau,\rho,\theta)$, after some calculations, Eq. (4.3) becomes

$$R(\tau,\rho,\theta) = I(\tau,\rho,\theta)\left((f^{cme}-\mathrm{i}f^{sme})(P^{-}f^{c}+\mathrm{i}P^{-}f^{s}) + (f^{cme}+\mathrm{i}f^{sme})(P^{+}f^{c}-\mathrm{i}P^{+}f^{s})\right). \tag{4.16}$$

We now set

$$\fint_{-\infty}^{\infty} \frac{f^c(\rho',\theta)}{\rho'-\rho}\mathrm{d}\rho' = h^c(\rho,\theta), \quad \fint_{-\infty}^{\infty} \frac{f^s(\rho',\theta)}{\rho'-\rho}\mathrm{d}\rho' = h^s(\rho,\theta),$$

thus Eq. (4.16) becomes

$$R(\tau,\rho,\theta) = -\mathrm{i}I(\tau,\rho,\theta)\left(f^{cme}\left(\frac{1}{\pi}h^c + 2f^s\right) + f^{sme}\left(\frac{1}{\pi}h^s - 2f^c\right)\right).$$

We denote the right–hand side of this equation by $-\mathrm{i}r(\tau,\rho,\theta)$. Taking the real part of $g(x_1,x_2)$ in (4.2), we obtain

$$g(x_1,x_2) = \frac{1}{4\pi}\int_0^{2\pi} \left(r_{x_1}\sin\theta - r_{x_2}\cos\theta\right)\mathrm{d}\theta, \tag{4.17}$$

where τ and ρ are given by (3.2) and

$$r(\tau,\rho,\theta) = I(\tau,\rho,\theta)\left(f^{cme}\left(\frac{1}{\pi}h^c + 2f^s\right) + f^{sme}\left(\frac{1}{\pi}h^s - 2f^c\right)\right). \tag{4.18}$$

For the numerical calculation of the Hilbert transform (4.8) we write

$$\begin{aligned} h(\rho,\theta) &= \fint_{-1}^{1} \frac{\hat f(\rho,\theta)}{\rho'-\rho}\mathrm{d}\rho' + \int_{-1}^{1} \frac{\hat f(\rho',\theta) - \hat f(\rho,\theta)}{\rho'-\rho}\mathrm{d}\rho' \\ &= \hat f(\rho,\theta)\ln\left(\frac{1-\rho}{1+\rho}\right) + \sum_{i=1}^{n-1}\int_{\rho_i}^{\rho_{i+1}} \frac{S_i(\rho',\theta) - \hat f(\rho,\theta)}{\rho'-\rho}\mathrm{d}\rho'. \end{aligned} \tag{4.19}$$

If $\rho = \rho_i$ or $\rho = \rho_{i+1}$ the integral in the right–hand side of (4.19) can be written

$$\int_{\rho_i}^{\rho_{i+1}} \frac{S_i(\rho',\theta) - S_i(\rho,\theta)}{\rho'-\rho}\mathrm{d}\rho'.$$

Thus, after some calculations, we obtain

$$\begin{aligned} &\int_{\rho_i}^{\rho_{i+1}} \frac{S_i(\rho',\theta) - \hat f(\rho,\theta)}{\rho'-\rho}\mathrm{d}\rho' = -\hat f_i + \hat f_{i+1} \\ &+\frac{1}{36}\left(4{\rho_i}^2 - 5\rho_i\rho_{i+1} - 5{\rho_{i+1}}^2 - 3(\rho_i - 5\rho_{i+1})\rho - 6\rho^2\right)\hat f_i'' \\ &+\frac{1}{36}\left(5{\rho_i}^2 + 5\rho_i\rho_{i+1} - 4{\rho_{i+1}}^2 - 3(5\rho_i - \rho_{i+1})\rho + 6\rho^2\right)\hat f_{i+1}''. \end{aligned} \tag{4.20}$$

If $\rho \neq \rho_i$ and $\rho \neq \rho_{i+1}$ the integral in the right–hand side of (4.19) can be written

$$\int_{\rho_i}^{\rho_{i+1}} \frac{S_i(\rho',\theta)}{\rho'-\rho}\mathrm{d}\rho' - \hat f(\rho,\theta)\ln\left|\frac{\rho_{i+1}-\rho}{\rho_i-\rho}\right|,$$

and after some calculation we obtain

$$\begin{aligned} h(\rho,\theta) &= \sum_{i=1}^{n-1}\left\{F_i - \frac{1}{\rho_i-\rho_{i+1}}\ln\left|\frac{\rho_{i+1}-\rho}{\rho_i-\rho}\right|\left[(\rho_{i+1}-\rho)\hat{f}_i - (\rho_i-\rho)\hat{f}_{i+1}\right.\right.\\ &- \left.\left.\frac{1}{6}(\rho_i-\rho)(\rho_{i+1}-\rho)\Big((\rho_i-2\rho_{i+1}+\rho)\hat{f}''_i + (2\rho_i-\rho_{i+1}-\rho)\hat{f}''_{i+1}\Big)\right]\right\}, \end{aligned} \tag{4.21}$$

where F_i is the right–hand side of (4.20).

In order to calculate numerically $I(\tau,\rho,\theta)$ for any x_1, x_2, θ, we use relation (4.7) and the second of relations (3.2). Thus

$$f(x_1,x_2) = -\frac{1}{4\pi^2}\int_0^{2\pi} h_\rho(x_2\cos t - x_1\sin t, t)\mathrm{d}t,$$

and consequently

$$F_\theta(\tau,\rho) = -\frac{1}{4\pi^2}\int_0^{2\pi} h_\rho(\tau\sin(\theta-t)+\rho\cos(\theta-t),t)\mathrm{d}t, \tag{4.22}$$

where τ and ρ are given from (3.2) and h_ρ from (4.11). We can now calculate $F_\theta(\tau,\rho)$ following the procedure outlined in the previous subsection. We then calculate $I(\tau,\rho,\theta)$ using relation (4.12) if $\tau \geq 0$, alternatively the relation

$$I(\tau,\rho,\theta) = \exp\left[\hat{f}(\rho,\theta) - \int_{-\sqrt{1-\rho^2}}^{\tau} F_\theta(\tau',\rho)\mathrm{d}\tau'\right] \tag{4.23}$$

if $\tau < 0$. For the numerical calculation of the integrals appearing in (4.12) and (4.23) we use the Gauss–Legendre quadrature with two functional evaluations at every step, i.e.

$$\int_\alpha^\beta F_\theta(\tau',\rho)\mathrm{d}\tau' \approx w_1F_\theta(\tau_1,\rho) + w_2F_\theta(\tau_2,\rho),$$

where the abscissas τ_1, τ_2 and the weights w_1, w_2 are given by

$$\tau_1 = \alpha + (\beta-\alpha)\left(\frac{1}{2}-\frac{\sqrt{3}}{6}\right), \quad \tau_2 = \alpha + (\beta-\alpha)\left(\frac{1}{2}+\frac{\sqrt{3}}{6}\right), \quad w_1 = w_2 = \frac{1}{2}(\beta-\alpha).$$

We also notice that we have tried subdivision of the interval (α,β) into several intervals and the improvement is very minor. Therefore we use just one interval, i.e. two function evaluations per quadrature, since the major increase in running time of the program implicit in using panel quadrature is not justified by the modest improvement in accuracy.

For the numerical calculation of the integrals in (4.17) and (4.22) we use again formula (4.9), resulting in spectral convergence. For the numerical calculation of the partial derivatives r_{x_1} and r_{x_2} in (4.17) we use the forward difference scheme

$$f'(x) \approx \frac{-3f(x) + 4f(x + \Delta x) - f(x + 2\Delta x)}{2\Delta x}$$

for the first half of the interval $[-1, 1]$, and the backward difference scheme

$$f'(x) \approx \frac{3f(x) - 4f(x - \Delta x) + f(x - 2\Delta x)}{2\Delta x}$$

for the second half.

Thus, for the numerical calculation of $g(x_1, x_2)$ from the data $\hat{f}(\rho, \theta)$ and $\hat{g}_f(\rho, \theta)$ we apply the following procedure: First we calculate the second derivatives $\hat{f}_i''$, using subroutine `spline`. Consequently, we calculate $h(\rho, \theta)$ using (4.19) and (4.20) for all given ρ and θ. We note that if $|\rho_i| = 1$, then, since we have assumed compact support, $\hat{f}(\rho, \theta) = 0$, thus the first term in (4.19) is absent. We then calculate $f^{cpe}(\rho, \theta)$ and $f^{spe}(\rho, \theta)$ using (4.13), as well as $f^c(\rho, \theta)$ and $f^s(\rho, \theta)$ using (4.15) (at this stage we use the second data function $\hat{g}_f$). Finally we calculate, again using `spline`, the second derivatives for the natural cubic spline interpolation of the functions $f^c(\rho, \theta)$ and $f^s(\rho, \theta)$.

Having calculated all the necessary second derivatives we now proceed as follows: First we calculate $\hat{f}(\rho, \theta)$ for any x_1, x_2 (and θ) using (3.2) and (4.10). For this purpose we have used subroutine `splint` from Numerical Recipes. Consequently we calculate $h(\rho, \theta)$ using (4.21). Then we calculate $f^{cme}(\rho, \theta)$ and $f^{sme}(\rho, \theta)$ using (4.14), $f^c(\rho, \theta)$ and $f^s(\rho, \theta)$ using `splint` and finally $h^c(\rho, \theta)$ and $h^s(\rho, \theta)$ using relations similar to (4.21). These last six functions are used in (4.18). We then calculate $I(\tau, \rho, \theta)$ as described earlier. Finally we calculate $r(\tau, \rho, \theta)$ using (4.18) and consequently $g(x_1, x_2)$ using (4.17).

4.2.3 Numerical results

The θ points are equally spaced in $[0, 2\pi]$, while the ρ points are equally spaced in $[-1, 1]$. The density plots presented below were drawn by using `Mathematica`. The dark color represents zero (or negative) values while the white color represents the maximum value of the function.

Here we present some numerical results for the NCAT phantom [Garrity et al., 2003]. This phantom provides a realistic model of the anatomy in the human thorax. In Fig. 3 four transversal cuts of this phantom are shown. These density plots represent the attenuation coefficient $f(x_1, x_2)$. In Fig. 4 the density plots of the relevant distribution function $g(x_1, x_2)$ are shown.

First we tested the CT algorithm for the four different cuts of the NCAT phantom, shown in Figs. 3. Using the Radon transform (3.4), we computed numerically the data function $\hat{f}(\rho, \theta)$ for 200 points for θ and 100 points for ρ. We then used these data in the numerical algorithm to re–evaluate $f(x_1, x_2)$. In order to remove the effect of the Gibbs–Wilbraham phenomenon, we applied an averaging filter as follows: We first found the maximum value (max) of $f(x_1, x_2)$ in the reconstructed image. We then set to zero those values of $f(x_1, x_2)$ which were less than $\frac{1}{15}$ max. Finally we applied the averaging filter with averaging parameter $a = 0.005$. This filtering procedure was applied five times, with the additional elimination of those values of $f(x_1, x_2)$ which were less than $\frac{1}{15}$ max at the end of the procedure. In Figs. 5 and 6 the results before and after the filtering procedure, respectively, are presented. The reconstruction took place in a 500×500 grid.

We then tested the SPECT algorithm for the four different cuts, shown in Figs. 4. By using the Radon transform (3.4), and the attenuated Radon transform (4.1), we computed numerically the data functions $\hat{f}(\rho, \theta)$ and $\hat{g}_f(\rho, \theta)$ for 200 values of θ and 100 points of ρ. We consequently used these data in our program to re–evaluate $g(x_1, x_2)$. In order to remove the effect of the Gibbs–Wilbraham phenomenon, a median filter was used, with the additional elimination of those values of $g(x_1, x_2)$ which were less than $\frac{1}{15}$ max before and after the application of the filter.

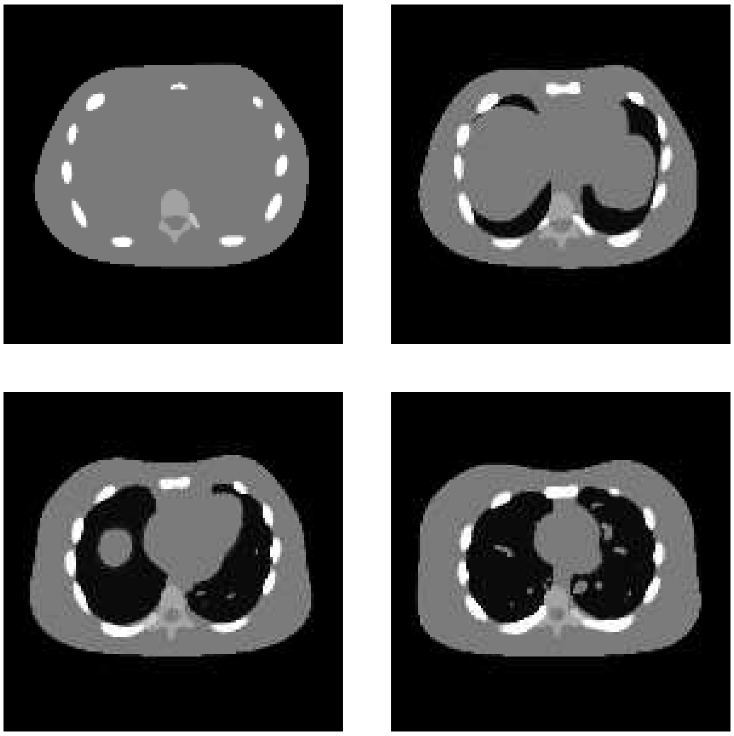

Figure 3: Four transversal cuts of the NCAT phantom depicting the x–ray attenuation coefficient $f(x_1, x_2)$.

The results are shown in Figs. 7 and 8, before and after the filtering procedure respectively. The reconstruction took place in a 140×140 grid.

Acknowledgments

A.S.F. was partially supported by the EPSRC. V.M. was supported by a Marie Curie Individual Fellowship of the European Community under contract number HPMF-CT-2002-01597. Some of the results presented here were jointly obtained with I.M. Gel'fand, Y. Kurylev and A. Iserles.

References

Andreasen, N. C. [1997] "Linking mind and brain in the study of mental illnesses: a project for a scientific psychopathology", *Sci.* **275**, 1586.

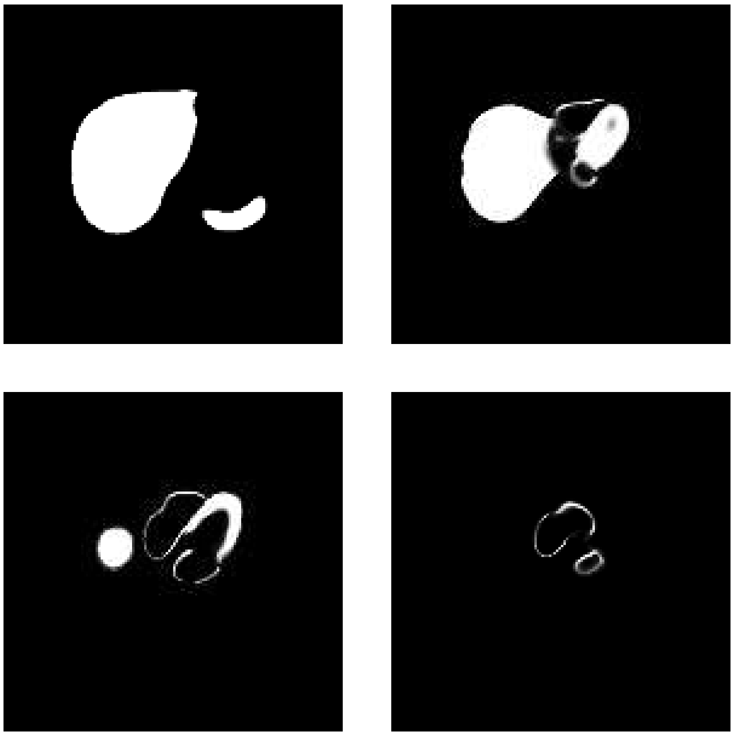

Figure 4: Four transversal cuts of the NCAT phantom depicting the distribution function $g(x_1, x_2)$ associated with the values of f shown in Figs. 3.

Bengel, F. M. et al. [2001] "Effect of sympathetic reinnervation on cardiac performance after heart transplantation", *N. Engl. J. Med.* **345**, 731.

Dassios, G. & Kariotou, F. [2003] "On the Geselowitz formula in biomagnetics", *Quar. Appl. Math.* **LXI**, 387–400.

Digital Equipment Corporation [1998] *Digital Visual Fortran, Version 6.0.*

Doubrovin, M. et al. [2001] "Imaging transcriptional regulation of p53–dependent genes with positron emission tomography in vivo", *Proc. Natl Acad. Sci. USA*, **98**, 9300.

Edelman, G. & Tononi, G. [2000] *A Universe of Consciousness: How Matter becomes Imagination* (Basic Books).

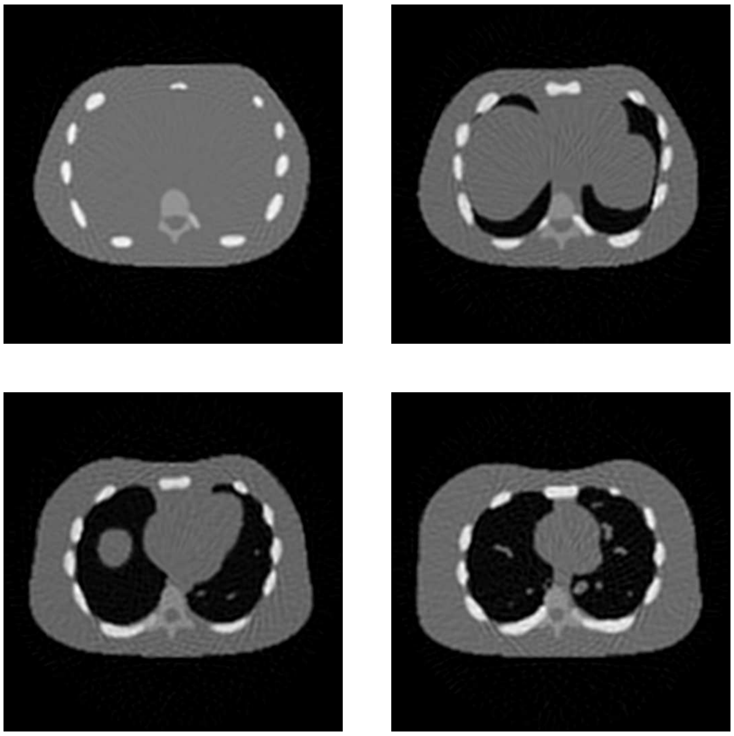

Figure 5: The reconstruction of the phantoms of Figs. 3 before the filtering procedure.

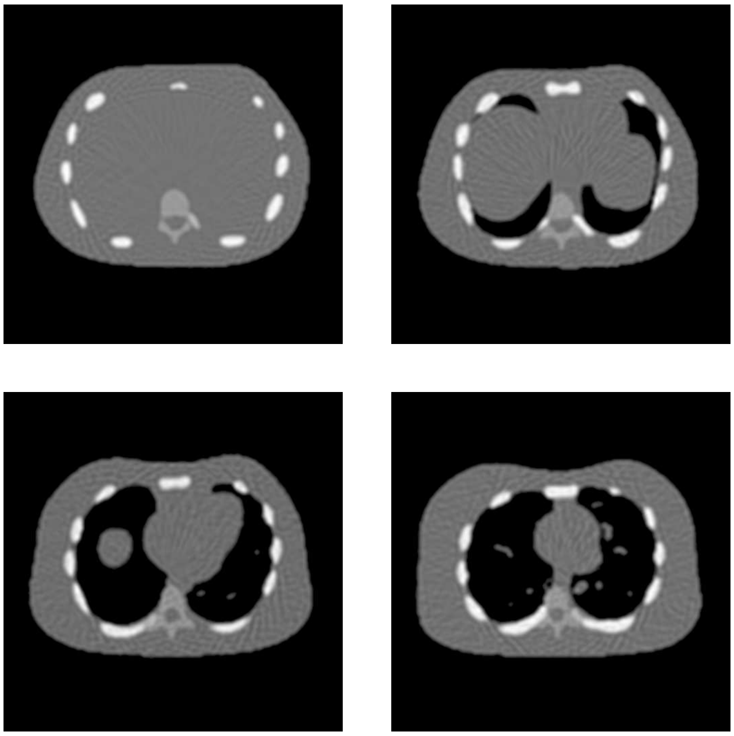

Figure 6: The reconstruction of the phantoms of Figs. 3 after the filtering procedure.

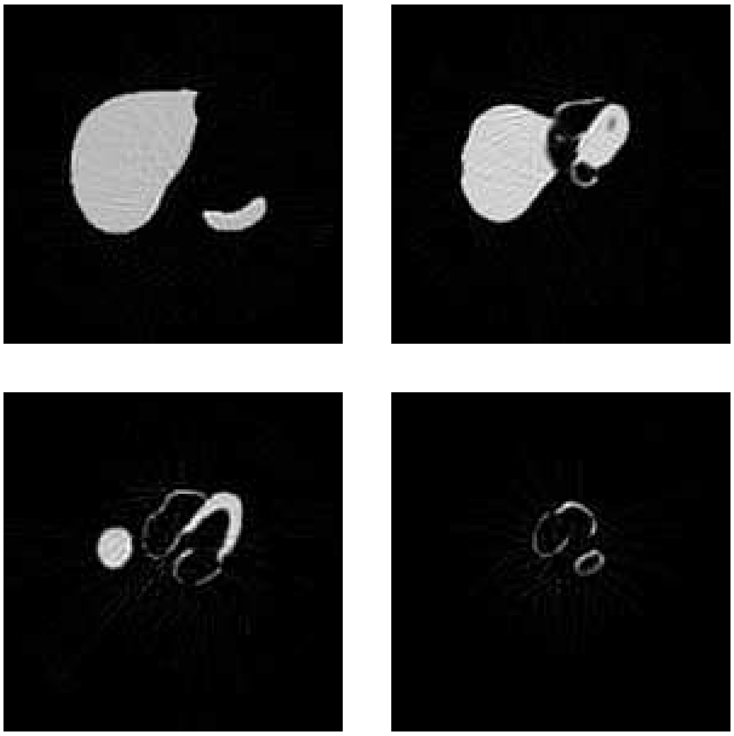

Figure 7: The reconstruction of the phantoms of Figs. 4 before the filtering procedure.

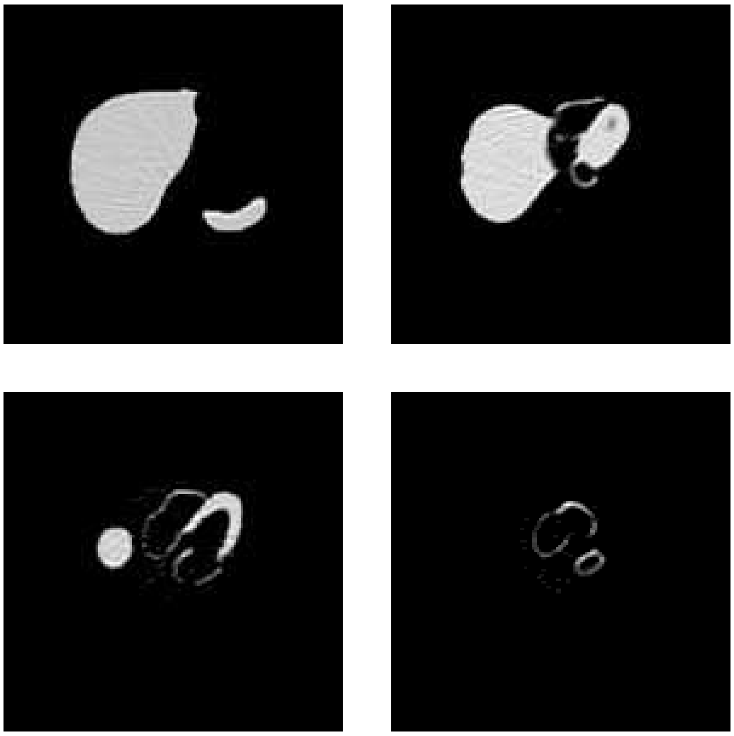

Figure 8: The reconstruction of the phantoms of Figs. 4 after the filtering procedure.

Fokas, A. S., Gel'fand, I. M. & Kurylev, Y. [1996] "Inversion method for magnetoencephalography", *Inv. Prob.* **12**, L9–L11.

Fokas, A. S., Kurylev, Y. & Marinakis, V. [2004a] "The unique determination of neuronal currents in the brain via magnetoencephalography", *Inv. Prob.* **20**, 1067–1082.

Fokas, A. S., Iserles, A. & Marinakis, V. [2004b] "Reconstruction algorithms for positron emission tomography and single photon emission computed tomography and their numerical implementation", preprint.

Fornberg, B. [1996] *A Practical Guide to Pseudospectral Methods* (Cambridge University Press).

Garrity, J. M., Segars, W. P., Knisley, S. B. & Tsui, B. M. W. [2003] "Development of a dynamic model for the lung lobes and airway tree in the NCAT phantom", *IEEE Trans. Nucl. Sci.* **50**, 378–383.

Geselowitz, D. B. [1970] "On the magnetic field generated outside an inhomogeneous volume conductor by internal current sources", *IEEE Trans. Magn.* **6**, 346–347.

Green, P. J. [1990] "Bayesian reconstruction from emission tomography data using a modified EM algorithm", *IEEE Trans. Med. Imag.* **9**, 84–93.

Green, L. A. et al. [2002] "Indirect monitoring of endogenous gene expression by positron emission tomography (PET) imaging of reporter gene expression in transgenic mice", *Mol. Imaging Biol.* **4**, 71.

Grynszpan, F. & Geselowitz, D. B. [1973] "Model studies of the magnetocardiogram", *Biophys. J.* **13**, 911–925.

Helmholtz, H. [1853] "Ueber einige gesetze der vertheilung elektrischer strome in korperlichen leitern mit anwendung auf diethierisch–elektrischen versuche (some laws about the distribution of electrical currents in volume conductors, with aplication to animal electric experiments)", *Ann. Phys. Chem.* **89**, 211–233 & 353–377.

Hille, B. [1992] *Ionic Channels of Excitable Membranes (2nd edition)* (Sinauer Associates, Massachusetts).

Hudson, H. M. & Larkin, R. S. [1994] "Accelerated image reconstruction using ordered subsets of projection data", *IEEE Trans. Med. Imag.* **13**, 601–609.

Hutton, B. F. [1997] "Cardiac single–photon emission tomography: is attenuation correction enough?" (invited editorial), *Eur. J. Nucl. Med.* **24**, 713.

Hutton, B. F., Hudson, H. M. & Beekman, F. J. [1997] "A clinical perspective of accelerated statistical recontruction", *Eur. J. Nucl. Med.* **24**, 797–808.

Ilmoniemi, R. J., Hamalainen, M. S. & Knuutila, J. [1985] "The forward and inverse problems in the spherical model", in *Biomagnetism: Applications and Theory*, eds. Weinberg, H., Stroink, G. & Katila, T. (Pergamon, New York).

Jonides, J. et al. [1996] "Verbal and spatial working memory in humans", *Psychol. Learn. Motiv.* **35**, 43.

Junck, L. et al. [1989] "PET imaging of human gliomas with ligands for the peripheral benzodiazepine binding site", *Ann. Neurol.* **26**, 752.

Koh, D., Cook, G. J. R. & Husband, J. E. [2003] "New horizons in oncologic imaging" (editorial), *N. Engl. J. Med.* **348**, 2487.

Kunyansky, L. A. [2001] "A new SPECT reconstruction algorithm based on the Novikov explicit inversion formula", *Inv. Prob.* **17**, 293–306.

Lalush, D. S. [2004] "Iterative image reconstruction", in *Emission Tomography: The Fundamentals of PET and SPECT*, eds. Wernick, M. & Aarsvold, J. (Academic Press, San Diego).

Lang, K. & Fessler, J. A. [1995] "Globally convergent algorithms for maximum a posteriori transmisson tomography", *IEEE Trans. Imag. Proc.* **4**, 1430–1438.

Lardinois, D. et al. [2003] "Staging of non–small–cell lung cancer with integrated positron–emission tomography and computed tomography", *N. Engl. J. Med.* **348**, 2500.

Lauritzen, M. & Olesen, J. [1984] "Regional cerebral blood flow during migraine attacks by xenon–133 inhalation and emission tomography", *Brain* **107**, 447.

Lee, B. I. et al. [1988] "HIPDM–SPECT in patients with medically intractable complex partial seizures: ictal study", *Arch. Neurol.* **45**, 397.

Mark, G. S. et al. [1996] "Understanding emotional prosody activates right hemisphere regions", *Arch. Neurol.* **53**, 665.

Mazziotta, J. C. [1992] "Movement disorders", in *Clinical Brain Imaging: Principles and Applications*, eds. Mazziotta, J. C. & Gilman, S. (Philadelphia: F. A. Davis) p. 244.

Mazziotta, J. C. et al. [1987] "Reduced cerebral glucose metabolism in asymptomatic subjects at risk for Huntington's disease", *N. Engl. J. Med.* **316**, 357.

Miller, M. I., Snyder, D. L. & Miller, T. R. [1985] "Maximum likelihood reconstruction for single–photon emision computed tomography", *IEEE Trans Nucl. Sci.* **32**, 769–778.

Minoshima, S. et al. [1995] "A diagnostic approach in Alzheimer's disease using three–dimensional stereotactic surface projections of fluorine–18–FDG PET", *J. Nucl. Med.* **36**, 1238.

Natterer, F. [2001] "Inversion of the attenuated Radon transform", *Inv. Prob.* **17**, 113–119.

Novikov, R. G. [2002] "An inversion formula for the attenuated x–ray transformation", *Ark. Mat.* **40**, 145.

Ost, D., Fein, A. M. & Feinsilver, S. H. [2003] "The solitary pulmonary nodule", *N. Engl. J. Med.* **348**, 2535.

Press, W. H., Teukolsky, S. A., Vetterling, W. T. & Flannery, B. P. [1992] *Numerical Recipes in Fortran. The Art of Scientific Computing (2nd edition)* (Cambridge University Press).

Reiman, E. M. et al. [1989] "Neuroanatomical correlates of anticipatory anxiety", *Sci.* **243**, 1071.

Sarvas, J. [1987] "Basic mathematical and electromagnetic concepts of the biomagnetic", *Inv. Prob. Phys. Med. Biol.* **32**, 11–22.

Shepp, L. A. & Vardi, Y. [1982] "Maximum likelihood reconstruction for emission tomography", *IEEE Trans. Med. Imag.* **1**, 113–122.

Tjuvajev, J. G. et al. [1999] "A general approach to the non–invasive imaging of transgenes using gis–linked herpes simplex virus thymidine kinase", *Neoplasia* **1**, 315.

Tyler, J. L. & Byme, T. N. [1992] "Neoplastic disorders", in *Clinical Brain Imaging: Principles and Applications*, eds. Mazziotta, J. C. & Gilman, S. (Philadelphia: F. A. Davis) p. 166.

Vorstrup, S., Paulson, O. B. & Lassen, N. A. [1986] "Cerebral blood flow in acute and chronic ischemic stroke using xenon–133 inhalation tomography", *Acta Neurol. Scand.* **74**, 439.

Wackers, F. J. T. [1999] "Attenuation correction, or the emperor's new clothes?" (editorial), *J. Nucl. Med.* **40**, 1310.

Wolfram, S. [1999] *The Mathematica Book (4th edition)* (Cambridge University Press).

Yu, Y. et al. [2000] "Quantification of target gene expression by imaging reporter gene expression in living animals", *Nature Med.* **6**, 933.

Appendix

In order to derive Eq. (3.12) we need to compute the limits of μ as λ tends to $\lambda^{\pm}$. As $\varepsilon \to 0$, (3.11) implies

$$\lambda^{+} \mp \frac{1}{\lambda^{+}} \sim (1-\varepsilon)\mathrm{e}^{\mathrm{i}\theta} \mp (1+\varepsilon)\mathrm{e}^{-\mathrm{i}\theta}.$$

Substituting this expression in the definition of z (Eq. (3.7)) and simplifying, we find

$$z' - z \sim (x_1' - x_1)\sin\theta - (x_2' - x_2)\cos\theta + \mathrm{i}\varepsilon((x_1' - x_1)\cos\theta + (x_2' - x_2)\sin\theta),$$

and rewriting the right–hand side of this equation in terms of the local coordinates ρ, ρ', τ, τ', we obtain

$$z' - z \sim -\rho' + \rho + \mathrm{i}\varepsilon(\tau' - \tau).$$

Substituting this expression in Eq. (3.9) and using the fact that the relevant sign equals 1, we find

$$\mu(x_1, x_2, \lambda^{+}) \sim -\frac{1}{2\pi\mathrm{i}} \iint\limits_{\mathbb{R}^2} \frac{f(x_1', x_2')\mathrm{d}x_1'\mathrm{d}x_2'}{\rho' - \rho - \mathrm{i}\varepsilon(\tau' - \tau)}, \quad \varepsilon \to 0, \quad \varepsilon > 0. \tag{1}$$

Using the change of variables $(x_1, x_2) \leftrightarrow (\tau, \rho)$ defined by Eqs. (3.1) and (3.2), and noting that the relevant Jacobian is 1, i.e.

$$f(x_1', x_2')\mathrm{d}x_1'\mathrm{d}x_2' = F_\theta(\tau', \rho')\mathrm{d}\tau'\mathrm{d}\rho',$$

we find that the right–hand side of Eq. (1) equals

$$-\frac{1}{2\mathrm{i}\pi} \iint\limits_{\mathbb{R}^2} \frac{F\mathrm{d}\tau'\mathrm{d}\rho'}{\rho' - (\rho + \mathrm{i}\varepsilon(\tau' - \tau))}. \tag{2}$$

In order to simplify this expression we split the integral over $\mathrm{d}\tau'$ in the form

$$\int_{-\infty}^{\infty} \mathrm{d}\tau' = \int_{-\infty}^{\tau} \mathrm{d}\tau' + \int_{\tau}^{\infty} \mathrm{d}\tau',$$

and note that in the first integral $\tau' - \tau < 0$, while in the second integral $\tau' - \tau > 0$. Thus, using the second set of Eqs. (3.13) the expression in (2) becomes

$$-\frac{1}{2\pi\mathrm{i}} \int_{-\infty}^{\infty} \left(\oint_{-\infty}^{\infty} F_\theta(\tau', \rho') \frac{\mathrm{d}\rho'}{\rho' - \rho} \right) \mathrm{d}\tau' - \frac{1}{2} \int_{\tau}^{\infty} F_\theta(\tau', \rho)\mathrm{d}\tau' + \frac{1}{2} \int_{-\infty}^{\tau} F_\theta(\tau', \rho)\mathrm{d}\tau'.$$

Finally, adding and subtracting the integral $\frac{1}{2}\int_\tau^\infty$ we find

$$\begin{aligned}\mu(x_1,x_2,\lambda^+) &= -\frac{1}{2\pi\mathrm{i}}\int_{-\infty}^{\infty}\left(\oint_{-\infty}^{\infty} F_\theta(\tau',\rho')\frac{\mathrm{d}\rho'}{\rho'-\rho}\right)\mathrm{d}\tau' \\ &\quad +\frac{1}{2}\int_{-\infty}^{\infty} F_\theta(\tau',\rho)\mathrm{d}\tau' - \int_\tau^\infty F_\theta(\tau',\rho)\mathrm{d}\tau'.\end{aligned}$$

The first two terms in the right–hand side of this equation equal $-P^-\hat{f}$, hence we find $(3.12)^+$.

The derivation of Eq. $(3.12)^-$ is similar.